ments; thin Mylar tape was used for the one window. Fluorescence was monitored in the direction normal to the incident x-ray beam in the horizontal plane. A single sample cell, extensively rinsed with an EDTA solution and deionized water between samples, was used for all the XRF measurements. Zn standards of 0, 0.5, 1.0, and 2.0 mM were prepared from a Zn atomic absorption standard solution (Sigma); solution volumes were measured gravimetrically. Data for the PKC βI and control samples and the Zn standard solutions were accumulated for 5 min each at room temperature. Raw data in the form of fluorescence counts versus MCA channel number were converted to counts versus energy with the Cr K_α peak (5.41 keV) and the scatter peak (11.2 keV) in a two-point linear calibration. Each of the energy-calibrated spectra was interpolated onto an evenly spaced energy grid and normalized by the integrated counts in the scatter peak to correct for differences in total incident flux. Difference spectra were computed for the Zn standards and the PKC βI sample (PKC βI − control), and the counts in the Zn K_α peaks were integrated. The standard deviation for the Zn concentration in the PKC βI sample was estimated from the results of different attempts at energy calibration, spectra normalization, and integration of the Zn counts.

17. The composition analysis, for which duplicate measurements were made on two different sample aliquots, gave a value of 29.2 ± 1.2 mg/ml for the total protein concentration. Coomassie blue–stained SDS-polyacrylamide gels (12.5%) (Fig. 2A) were scanned (two dimensionally) with a Molecular Dynamics densitometer to obtain an estimate of the percentage of protein that was PKC βI. Several lanes with differing amounts of loaded protein were analyzed. The PKC βI band comprised 76 ± 4% of the total stained protein. The next highest intensity band was ~4% of the total.

18. Fluorescence EXAFS data for the PKC βI sample were taken at ~15 K. Twenty-one scans, each 35 min in duration, were recorded with step sizes of 2.0 and 3.0 eV in the EXAFS region. Because of a small amount of contaminating W in the He cryostat, the usable data range was limited to <10.2 keV. Two scans to be used for baseline subtraction were taken of the cell containing sample buffer. The monochromator crystals were detuned to 42% to suppress higher energy harmonics. A Zn foil placed downstream of the sample position was used to calibrate the energy; 9.661 keV was assigned to the K-edge inflection point. Averaged sample spectra were computed; the data from each Ge element of the detector array were weighted by the size of the edge jump. The baseline spectrum showed a small Zn K-edge feature (edge jump was 14% of that of the PKC βI sample) due to a contaminant in the cryostat. The baseline spectrum was smoothed, retaining the edge feature, and subtracted from the PKC βI spectrum. A cubic spline was fit to the region above the edge to extract the EXAFS oscillations. Conversion from energy E (keV) to photoelectron wave number k ($Å^{-1}$) was done with an estimate for the threshold energy, E_0, of 9.670 keV [$k = \sqrt{0.262(E - E_0)}$]. EXAFS spectra were smoothed with a Gaussian function of width 0.1 $Å^{-1}$. Transmission EXAFS data for a Zn model compound, (1,10-phenanthroline)bis(4-toluenethiolato)Zn^{2+} [T. L. Cremers, D. R. Bloomquist, R. D. Willet, G. A. Crosby, *Acta Crystallogr. B* **36**, 3097 (1980)], in the form of a sucrose-diluted fine powder, were taken at room temperature.

19. S. P. Cramer and K. O. Hodgson, *Prog. Inorg. Chem.* **25**, 1 (1979).
20. J. J. Rehr, J. Mustre de Leon, S. I. Zabinsky, R. C. Albers, *J. Am. Chem. Soc.* **113**, 5135 (1991).
21. Discriminating between an N and an O backscatterer is difficult, especially when the contribution of the low-Z ligand to the EXAFS is minor. In favorable cases, the backscattering contributions (from single and multiple scattering) from the outer C and N atoms of the His imidazole group are clearly observable [S. S. Hasnain and R. W. Strange, in *Synchrotron Radiation and Biophysics*, S. S. Hasnain, Ed. (Wiley, New York, 1990), chap. 4]. The analysis program EXCURV90 [N. Binstead, J. W. Campbell, S. J. Gurman, P. C. Stephenson, *SERC Dares-*

bury Laboratory EXCURV90 Program (1990)] was used to simulate single and multiple-scattering contributions from a single imidazole among three S backscatterers. The results indicated that the outer shell imidazole contributions would likely be obscured in experimental data.

22. In an initial XRF experiment with a less pure and less concentrated PKC βI sample, isolated in the presence of 0.5 mM EGTA and 0.5 mM EDTA (K_D for Zn^{2+} is $10^{-16.4}$ M), a Zn^{2+} to PKC βI stoichiometry of 3.1 ± 0.7 was obtained. We conclude from the two XRF results that in the presence of 1 mM EGTA all of the high affinity Zn^{2+} sites are loaded.

23. An assay to detect the presence of inorganic sulfide was performed according to the procedures of T. E. King and R. O. Morris [*Methods Enzymol.* **10**, 634 (1967)]. Using sodium sulfide and red algae ferredoxin (Sigma) as standards, we determined the amount of sulfide in the PKC βI sample to be <0.1 mol per mol of PKC βI.

24. Although pentacoordination by S and N atoms is found in bioinorganic Zn^{2+} compounds, in those cases examined one or more Zn–S distances are longer than the average Zn–S distance by at least 0.25 Å [T. P. E. Auf der Heyde and L. R. Nassimbeni, *Acta Crystallogr. B* **40**, 582 (1984)]. No evidence for a long S ligand is found in the EXAFS data.

25. A. H. Robbins et al., *J. Mol. Biol.* **221**, 1269 (1991).

26. S. S. Hasnain et al., *Experientia Suppl.* **52**, 227 (1987).
27. J. A. Tainer, E. D. Getzoff, K. M. Beem, J. S. Richardson, D. C. Richardson, *J. Mol. Biol.* **160**, 181 (1982).
28. J. F. Povey, G. P. Diakun, C. D. Garner, S. P. Wilson, E. D. Laue, *FEBS Lett.* **266**, 142 (1990).
29. T. Pan and J. E. Coleman, *Biochemistry* **29**, 3023 (1990).
30. A. D. Watson, C. P. Rao, J. R. Dorfman, R. H. Holm, *Inorg. Chem.* **24**, 2820 (1985).
31. T. K. Eccles, thesis, Stanford University (1977); modifications to the program were made by G. N. George (Exxon Research) and S.P.C.
32. Single-letter abbreviations for the amino acid residues are as follows: A, Ala; C, Cys; D, Asp; E, Glu; F, Phe; G, Gly; H, His; I, Ile; K, Lys; L, Leu; M, Met; N, Asn; P, Pro; Q, Gln; R, Arg; S, Ser; T, Thr; V, Val; W, Trp; and Y, Tyr.
33. We gratefully acknowledge J. Petrin's role in the PKC βI purification and the contributions of G. M. Housey and I. B. Weinstein to the cloning and overexpression of PKC βI. We benefited from discussions with G. N. George, R. A. Scott, B. Hedman, and K. O. Hodgson on EXAFS matters, and we thank W. Orme-Johnson for helpful suggestions on the inorganic sulfide assay. The Zn model compound was kindly provided by G. A. Crosby.

29 August 1991; accepted 30 October 1991

Novel Fold and Putative Receptor Binding Site of Granulocyte-Macrophage Colony-Stimulating Factor

KAY DIEDERICHS, TOM BOONE, P. ANDREW KARPLUS*

Granulocyte-macrophage colony-stimulating factor (GM-CSF) stimulates the development of and the cytotoxic activity of white blood cells. Recombinant human GM-CSF has proven useful in the treatment of blood disorders. The structure of GM-CSF, which was determined at 2.4 angstrom resolution by x-ray crystallography, has a novel fold combining a two-stranded antiparallel β sheet with an open bundle of four α helices. Residues implicated in receptor recognition, which are distant in the primary sequence, are on adjacent α helices in the folded protein. A working model for the receptor binding site is presented.

NATURAL GM-CSF IS A 127–AMINO acid residue trace glycoprotein (1, 2) that triggers the development of both granulocyte and macrophage colonies from hematopoietic progenitor cells (3). The availability of recombinant GM-CSF (2, 4, 5) has allowed a much fuller characterization of its activities, and it is now clear that GM-CSF stimulates a wide variety of hematopoietic and nonhematopoietic cell types (6). As a therapeutic agent, GM-CSF has shown promise in the treatment of aplastic anemia, myelodysplastic syndromes, acquired immune deficiency syndrome, neutropenias, and chemotherapy-induced myelosuppression (7, 8). As a step toward understanding its structure-function rela-

tions, we have crystallized nonglycosylated recombinant human GM-CSF (9). Here we report the structure at 2.4 Å resolution and define a putative receptor binding site.

The tertiary structure of GM-CSF is dominated by a bundle of four α helices and is distinctly nonspherical with dimensions of 20 Å by 30 Å by 40 Å (Fig. 1). The four helices are all antiparallel and form a twisted open barrel, with the open edge filled in by strand 1 of the antiparallel sheet. Each of the helices interacts with both of its neighbors around the barrel perimeter (Table 1) so that despite the presence of the β sheet, GM-CSF can be compared with known four-helix bundle proteins (10). The topology of the bundle places helices A and B, and helices C and D across the barrel from each other rather than next to each other. This placement gives GM-CSF a double overhand topology (10), which has previously been seen for porcine growth hormone (11). Although interesting, the simi-

K. Diederichs and P. A. Karplus, Section of Biochemistry, Molecular and Cell Biology, Cornell University, Ithaca, NY 14853.
T. Boone, AMGEN, Thousand Oaks, CA 91320–1789.

*To whom correspondence should be addressed.

larity to growth hormone does not extend to other key features of the GM-CSF fold, including the manner in which the helices pack together and the association of the two long overhand connections to build an antiparallel β sheet. Growth hormone has long helices (20 to 30 residues) that pack with all interhelical angles close to 180°, whereas the GM-CSF helices are only between 10 and 16 residues long and cross at angles up to

43° from perfect alignment (Table 1).

For these reasons, the GM-CSF structure is clearly distinct from that of growth hormone and represents a novel fold. The topology of the GM-CSF fold as a whole is reminiscent of the β-jellyroll member of the greek-key β-barrel family (12), with four of the sheet strands replaced by helices (Fig. 1B). Interestingly, the swirl of the GM-CSF jellyroll is left-handed, whereas all known

β-jellyrolls are right-handed. The two disulfide bonds in GM-CSF are both at the same end of the molecule and connect helix B to strand 2 of the β sheet and helix C to the carboxyl terminus, respectively. Although there are no topological loop crossings, the loop from residues 43 to 54 penetrates the macrocycle formed by the carboxyl-terminal disulfide (Cys^{88}-Cys^{121}) to result in a rare "threaded" topology (13). A conserved proline-rich sequence (residues 89 to 94; Fig. 2) adopts an extended conformation and makes key hydrogen bonds to stabilize the threaded interaction: the carbonyl of Pro^{92} hydrogen bonds to the amide of Cys^{54} and the carboxylate of Glu^{93} hydrogen bonds to amides of both Glu^{56} and Thr^{57} at the amino terminus of helix B.

Another notable feature of the fold is a stretch of 3_{10} helix from residues 68 to 73. The Pro^{76} residue interrupts the helical hydrogen-bonding pattern and causes a 30° bend in the chain leading into helix C. Since Pro^{76} is not conserved across species (Fig. 2), it is unclear whether the bend is also present in murine GM-CSF or whether helix C might be longer.

The solvent accessibility of each residue in GM-CSF (Fig. 2) is useful for distinguishing those residues that contribute to structural integrity from those that may be directly involved in receptor recognition. We can use the GM-CSF structure to show that many mutation studies aimed at characterizing structure-function relations for GM-CSF have been effective at locating structurally important regions rather than the receptor recognition site. A study of mutants in which various tripeptide deletions were made identified four regions in murine GM-CSF that were essential for activity (residues 18 to 22, 37 to 44, 54 to 64, and
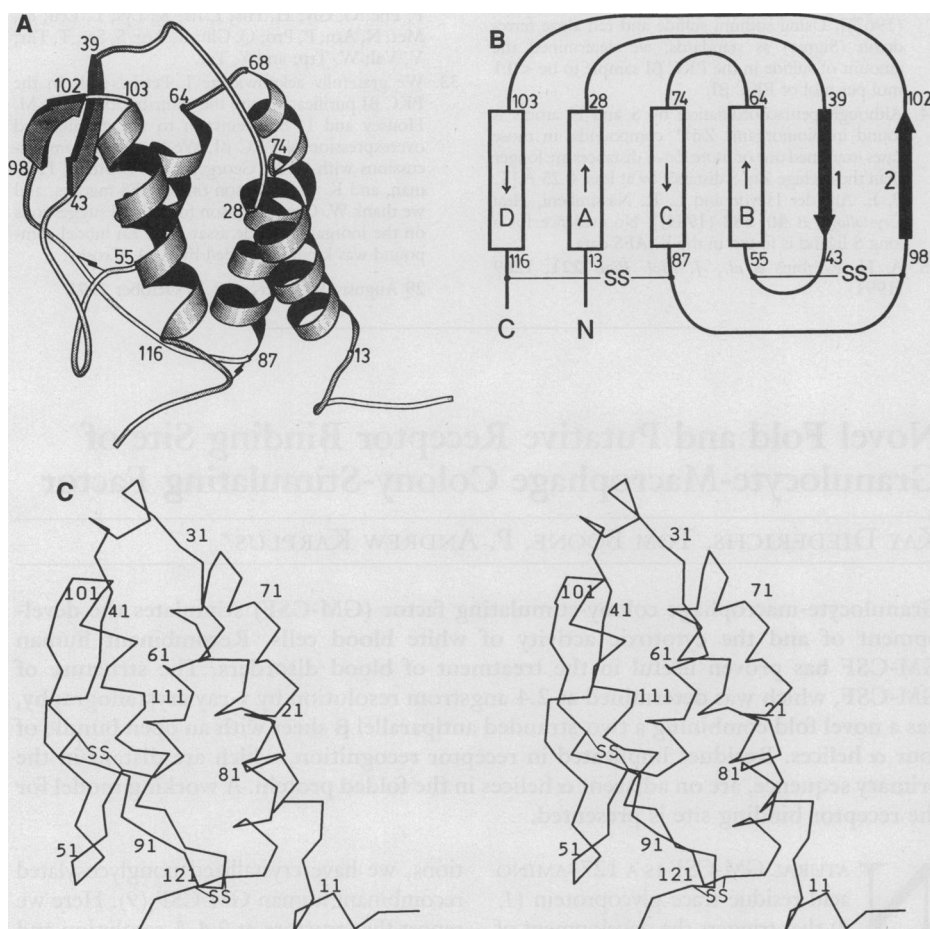

Fig. 1. The three-dimensional structure of GM-CSF. (**A**) A ribbon diagram (23) highlighting the secondary structural elements (24): helices are shown as spirals, β strands as arrows, and disulfides as lightning bolts. (**B**) Topology diagram showing the α/β-jellyroll topology. Rectangles represent helices (A, B, C, and D), and arrows represent β strands (1 and 2). The N and C mark the termini, and the disulfides are indicated. (**C**) A stereo Cα diagram with every tenth residue labeled and disulfides indicated. The view is the same as in (A). The loops at residues 31 to 38 and 45 to 52 have high mobility. Crystals of recombinant human GM-CSF ($P2_12_12_1$; $a = 47.6$, $b = 59.1$, and $c = 126.7$ Å) were grown and diffraction data were collected at room temperature on a San Diego Multiwire Systems detector (25) as described in the low-resolution structure determination (9). Two additional heavy-atom derivatives were found (mersalyl acid and HgI_2) that allowed better experimental phases to be determined. The multiple isomorphous replacement phases were refined by iterative solvent flattening (26) combined with noncrystallographic symmetry averaging (9) to yield a 3.5 Å resolution averaged electron density map that showed the characteristic spiral of the α helices and density for many side chains. One of the helices showed three large side chains pointing into the protein core and could be fit by residues 99 to 116, which include three Phe residues. No other parts of the sequence could be recognized in the electron density. After three rounds of model building and simulated annealing refinement (27) with the use of partial models, the electron density improved so that the true amino acid sequence could be assigned to the density. Five further cycles of model building and refinement were carried out and eventually used all of the data between 10 and 2.4 Å resolution to yield an R factor of 0.205. Individual atomic temperature factors were restrained, and the model has root-mean-square (rms) deviations from ideal geometry of 0.017 for bond lengths and 3.5° for bond angles. The two molecules related by noncrystallographic symmetry have an rms deviation of 1.2 Å for all atoms. The current model includes residues 5 through 123 of the protein and 64 bound water molecules. All model building was done on an Hewlett-Packard 9000/835 Workstation with the program FREIBAU (28).

Table 1. Geometry of the GM-CSF helix-packing interactions. The interhelix packing angle Ω is the angle between the vectors defining the directions of the two helices (10). A negative angle means the front helix of the pair is rotated clockwise relative to the back helix. The separation is the closest approach of the two axial vectors. Presnell and Cohen (10) also assessed the compactness of a helical bundle by the amount of surface area that became buried as each helix associated with the other three helices. For GM-CSF these numbers are 24, 21, 37, and 24% of the total accessible surface area of the four helices (= 4400 Å²), showing that the helices interact quite tightly with one another.

Helix pair	Separation (Å)	Ω (degrees)
A:C	8.4	−147
C:B	9.5	−171
B:D	11.4	−137
D:A	10.3	−148

Fig. 2. Secondary structure and solvent accessibility in human GM-CSF (*29*). Line 1 documents the accessibility ("acc" in Å^2) of each residue: ○ for acc > 50; ◑ for 20 < acc < 50; ● for acc < 20. Line 2 gives the sequence of the human GM-CSF used in this study (*30*), line 3 gives the sequence of murine (*5*) GM-CSF (dots

```
              10        20        30        40        50        60        70
               |         |         |         |         |         |         |
     ○○○○○○○○●○○●○○○●○●○○○○●○○○○○○○○●○○○●○○○○○○○○●○●●○●○○●○○●●●●●●○○●○●●○○●○●●
     APARSPSPSTQPWEHVNAIQEARRLLNLSRDTAAEMNETVEVISEMFDLQEPTCLQTRLELYKQGLRGSL
     ..T...ITV.R..K..E..K..IN..DDMPVTL---..E...V.NE.SFKKL..V....KIFE.....NF
       TTT   HHHHHHHHHHHHHH    HHHHT EEEEESS     TTS  SHHHHHHHHHT  GGG

              80        90       100       110       120
               |         |         |         |         |
     ○○○●●○●○○○●●●○○○●○○●○○○○○○○○○○○●●○○○●○○●○○○●●○○●○○○○○●○○○○
     TKLKGPLTMMASHYKQHCPPTPETSCATQIITFFESFKENLKDFLLVIPFDCWEPVQE
     .....A.N.T..Y.QTY.......D.E..VT.YAD.IDS..T..TD...E.KK.S.K
     GGGHHHHHHHHHHHHHS  SS  EEEEEHHHHHHHHHHHHHHS SS
```

indicate identities with human GM-CSF) and line 4 shows the secondary structure: *H*, α helix; *E*, β sheet; *G*, 3_{10} helix; *T*, turn; and *S*, bend. The human numbering used throughout the text is given. Secondary structures and accessible surface areas were calculated with the program DSSPNOV (*24*). The gap in murine GM-CSF is placed so as to least disrupt the path of the chain.
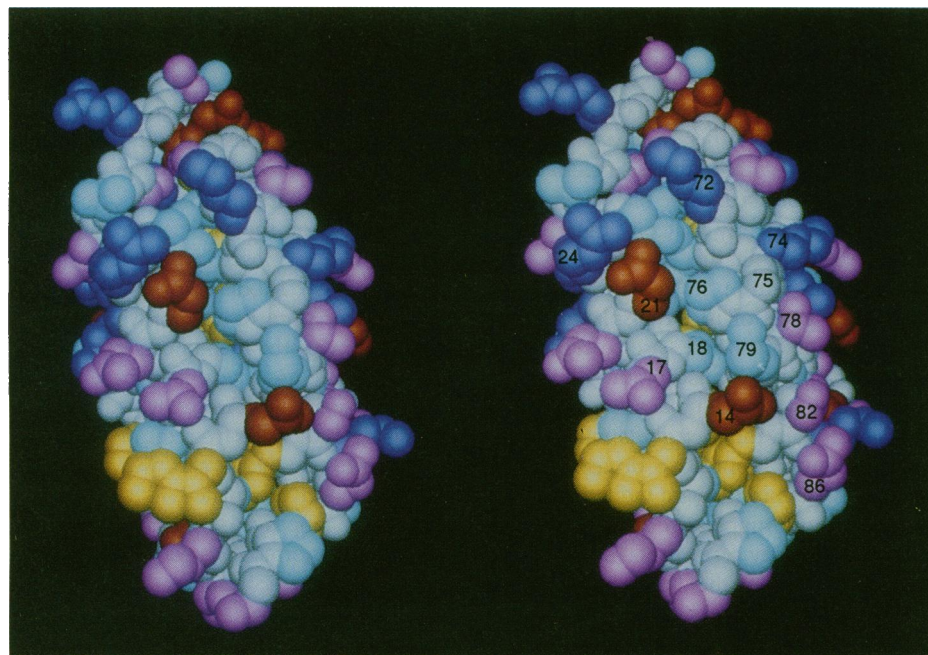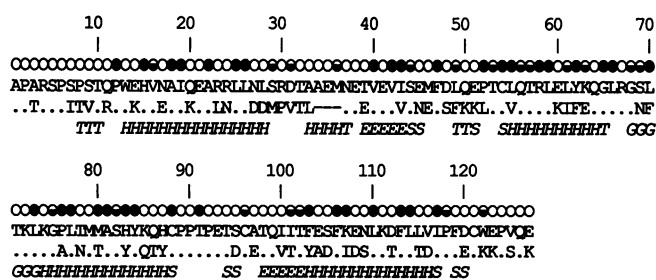

Fig. 3. A stereo view of the putative receptor binding site of GM-CSF. The view of GM-CSF shown is from the right-hand side of Fig. 1C and shows the narrow dimension of the molecule. The main chain is white, and side-chain colors are determined by residue type: apolar (G, A, P, C, V, I, L, and M), light blue; polar (S, T, N, and Q), purple; aromatic (H, F, Y, and W), yellow; negatively charged (D and E), red; and positively charged (K and R), blue. Residues defining the putative recognition site are labeled by residue number. Asn^{27} is just visible to the left of Arg^{24}, and a portion of Arg^{23} can be seen just below Asn^{27}. Image generated by the program BRAGI (*31*).

96 to 118; human numbering) (*14*). These four regions correspond to helix A, β strand 1, helix B, and a stretch including β strand 2 and helix D (Fig. 2). These regions are all likely to be critical for structural reasons and thus do not shed light on the receptor binding site. In another mutagenesis study, residues 17, 21, 38, 41, 46, 59, 63, 65, 104, and 110 of murine GM-CSF (human numbering) were individually mutated to Pro residues (*15*). Again, comparison with the GM-CSF structure shows that only the mutations in α helices, where a Pro would cause structural disturbance (residues 21, 59, 63, 66, and 110), showed drastic activity loss. Other GM-CSF mutants that had near wild-type activity indicate that residues 1 to 16, 67 to 70, 121 to 127, and the carboxyl-

terminal disulfide do not play key roles in either stability or recognition (*14, 16*).

In contrast, an approach that takes advantage of the fact that human and murine GM-CSF are species-specific has identified key residues that are not structurally crucial. Assuming that equivalent regions of the murine and human GM-CSF are recognized by their receptors, Kaushansky *et al.* (*17*) used a series of chimeric human-murine GM-CSF molecules to show that residues 21 to 31 and 78 to 94 are important recognition regions. With residues 21 to 31 of murine GM-CSF replaced by the human counterpart, the hybrid no longer binds to the murine receptor, and the hybrid with residues 78 to 94 of human GM-CSF replaced by the murine sequence no longer binds to the human recep-

tor. Because residues 88 to 94 are conserved between murine and human GM-CSF, the second implicated region can be redefined as 78 to 87. Two further constructs pointed to the importance of Arg^{23} or Arg^{24} or both, because an Arg^{23} to Gln mutant of human GM-CSF showed a 75% loss in specific activity and because inserting an Arg-Arg-Leu tripeptide after residue 22 of murine GM-CSF (which puts it in registry with the human sequence) decreased its activity by 98%. Further evidence consistent with the importance of residues 21 to 31 is the observation that deglycosylation of Asn^{27}, which is adjacent to Arg^{24} on the surface of GM-CSF (Fig. 3), and Asn^{37} gives a 20-fold increase in the specific activity of GM-CSF (*18*), as if one or both of the carbohydrate groups interfere with receptor binding.

Although some of the results seen for the hybrid proteins may be indirect effects due to changes in protein conformation, it is interesting that residues 21 to 31 and 78 to 87 are mostly in helix A and helix C, which are neighbors in the helical bundle (Fig. 1). Residue 76 is spatially adjacent to residue 21, but as the helices are antiparallel, the two stretches of residues diverge from each other so that residue 87 is 35 Å from residue 31. Focusing on those implicated residues that are near each other allows us to present a putative receptor's view of the surface of GM-CSF centering on Arg^{24} and Met^{79} (Fig. 3). Ala^{18}, Gly^{75}, Pro^{76}, and Met^{79} form a hydrophobic patch surrounded by the polar side chains of Glu^{14}, Asn^{17}, Glu^{21}, Arg^{24}, Lys^{72}, Lys^{74}, Thr^{78}, Ser^{82}, and Gln^{86}. That residues 1 to 16 and the turn at 67 to 70 are not important for activity suggests the recognition site stops before Glu^{14} and does not extend above Lys^{72}. In addition to accounting for the available data, this proposed receptor recognition site also meshes nicely with ideas on protein-protein recognition, which suggest that hydrophobic groups are present to give strength to the interaction and hydrophilic groups to give the required specificity (*19*). Methodical mutagenesis of these surface residues should allow further delineation of the receptor recognition site or sites, and if receptor binding can truly be localized to residues from these two segments alone, it gives a reasonable hope that synthetic mimics of this surface may be developed.

The high-affinity (dissociation constant K_d = 30 pM) GM-CSF receptor on hematopoietic cells, which is formed when the 80-kD receptor combines with a 120-kD chain (*20*), has recently been shown to be a member of a family of structurally related receptors that includes the receptors for interleukin-2 and growth hormone (*21*). It is striking that GM-CSF, interleukin-2 (*22*), and growth hormone (*11*) have nonhomol-

ogous structures and thus apparently have evolved their receptor binding activities independently. The one thing that appears common to these structures is the high helical content and the use of residues in α helices for receptor binding.

Note added in proof: The secondary structure and topology of the cytokine interleukin-4 have been determined by nuclear magnetic resonance studies and it appears to have the same fold as GM-CSF (*32*).

REFERENCES AND NOTES

1. J. C. Gasson *et al.*, *Science* **226**, 1339 (1984).
2. G. G. Wong *et al.*, *ibid.* **228**, 810 (1985).
3. S. C. Clark and R. Kamen, *ibid.* **236**, 1229 (1987).
4. A. W. Burgess *et al.*, *Blood* **69**, 43 (1987); D. Metcalf, *Science* **254**, 529 (1991).
5. N. M. Gough *et al.*, *Nature* **309**, 763 (1984).
6. J. C. Gasson, *Blood* **77**, 1131 (1991).
7. M. A. S. Moore, *Annu. Rev. Immunol.* **9**, 159 (1991).
8. K. M. Sakamoto, D. W. Golde, J. C. Gasson, *J. Pediatr.* **118**, S17 (1991).
9. K. Diederichs, S. Jacques, T. Boone, P. A. Karplus, *J. Mol. Biol.* **221**, 55 (1991).
10. S. R. Presnell and F. E. Cohen, *Proc. Natl. Acad. Sci. U.S.A.* **86**, 6592 (1989).
11. S. S. Abdel-Meguid *et al.*, *ibid.* **84**, 6434 (1987).
12. J. S. Richardson, *Adv. Prot. Chem.* **34**, 167 (1981).
13. T. Creighton, in *Proteins: Structures and Molecular Properties* (Freeman, New York, 1984), pp. 226–227.
14. A. B. Shanafelt and R. A. Kastelein, *Proc. Natl. Acad. Sci. U.S.A.* **86**, 4872 (1989).
15. S. W. Altman, G. D. Johnson, M. B. Prystowky, *J. Biol. Chem.* **266**, 5333 (1991).
16. I. Clark-Lewis *et al.*, *J. Immunol.* **141**, 881 (1988).
17. K. Kaushansky, S. G. Shoemaker, S. Alfaro, C. Brown, *Proc. Natl. Acad. Sci. U.S.A.* **86**, 1213 (1989).
18. P. Moonen, J. J. Mermod, J. F. Ernst, M. Hirshi, J. F. DeLamarter, *ibid.* **84**, 4428 (1987).
19. J. Janin and C. Chothia, *J. Mol. Biol.* **100**, 197 (1976).
20. K. Hayashida *et al.*, *Proc. Natl. Acad. Sci. U.S.A.* **87**, 9655 (1990).
21. J. F. Bazan, *ibid.* **87**, 6934 (1990).
22. B. J. Brandhuber, T. Boone, W. C. Kenney, D. B. McKay, *Science* **238**, 1707 (1987).
23. P. J. Kraulis, *J. Appl. Crystallogr.*, **24**, 946 (1991).
24. W. Kabsch and C. Sander, *Biopolymers* **22**, 2577 (1983).
25. R. Hamlin, *Methods Enzymol.* **114**, 416 (1985).
26. B. C. Wang, *ibid.* **115**, 90 (1985).
27. A. T. Brünger, J. Kuriyan, M. Karplus, *Science* **235**, 458 (1987).
28. P. A. Karplus, M. J. Daniels, J. R. Herriott, *ibid.* **251**, 60 (1991).
29. Abbreviations for the amino acid residues are: A, Ala; C, Cys; D, Asp; E, Glu; F, Phe; G, Gly; H, His; I, Ile; K, Lys; L, Leu; M, Met; N, Asn; P, Pro; Q, Gln; R, Arg; S, Ser; T, Thr; V, Val; W, Trp; and Y, Tyr.
30. S. Miyatake, T. Otsuka, T. Yokota, F. Lee, K. Arai, *EMBO J.* **4**, 2561 (1985).
31. D. Schomburg and J. Reichelt, *J. Mol. Graphics* **6**, 161 (1988).
32. C. Redfield *et al.*, *Biochemistry* **30**, 11029 (1991).
33. The complete refined coordinate set for GM-CSF has been deposited in the Brookhaven Protein Data Bank (entry 1 GMF). K.D. thanks the Alexander von Humboldt Foundation (Bonn) for a postdoctoral fellowship. We thank S. Jacques for growing crystals and the Hewlett-Packard Corporation for donating the graphics workstation. Supported by a grant from the Cornell Biotechnology Program, which is sponsored by the New York State Science and Technology Foundation, a consortium of industries, the U.S. Army Research Office, and the National Science Foundation.

27 September 1991; accepted 1 November 1991

Maintenance of Normoglycemia in Diabetic Mice by Subcutaneous Xenografts of Encapsulated Islets

PAUL E. LACY,* ORION D. HEGRE, ANDRIANI GERASIMIDI-VAZEOU, FRANK T. GENTILE, KEITH E. DIONNE

The goal of islet transplantation in human diabetes is to maintain the islet grafts in the recipients without the use of immunosuppression. One approach is to encapsulate the donor islets in permselective membranes. Hollow fibers fabricated from an acrylic copolymer were used to encapsulate small numbers of rat islets that were immobilized in an alginate hydrogel for transplantation in diabetic mice. The fibers were biocompatible, prevented rejection, and maintained normoglycemia when transplanted intraperitoneally; hyperglycemia returned when the fibers were removed at 60 days. Normoglycemia was also maintained by subcutaneous implants that had an appropriately constructed outer surface on the fibers.

SERIOUS COMPLICATIONS INVOLVING the eyes, kidneys, and cardiovascular and peripheral nervous systems occur in individuals with diabetes mellitus. Although controversial, these diabetic complications are apparently related to the inability of exogenous insulin therapy to maintain the blood sugar within normal limits at all times. The goals of islet transplantation in the treatment of diabetes are to transplant islets early in the course of the disease in order to achieve continuous normoglycemia and to maintain the islet grafts without the use of immunosuppressive drugs. Human islet transplants in diabetic individuals who receive immunosuppressive drugs for maintenance of kidney transplants can produce normoglycemia in the recipients without exogenous insulin (*1*). The ideal immunoisolatory device for transplantation of islets in diabetic individuals would be biocompatible, maintain the viability and normal function of the islets, prevent cellular immune rejection, exclude antibodies to islet cells, maintain normoglycemia in the recipients, contain sufficient numbers of islets, be implanted either intraperitoneally or subcutaneously, and be easily and safely retrieved if desired.

Islet allograft rejection has been prevented without immunosuppression by isolating the islets from the immune system of the recipients with permselective membranes. Alginate (a naturally occurring linear polysaccharide extracted from kelp containing D-mannuronic and L-guluronic acid monomeric units) was cross-linked with Ca^{2+} to form a hydrogel. Encapsulation of individual islets in microspheres of alginate hydrogel with a coating of poly(L-lysine) produced

a slight prolongation of intraperitoneal implants of encapsulated rat islet allografts (*2*). The capsules were insufficiently stable and biocompatible, a large volume of encapsulated islets was needed to achieve normoglycemia, and all of the encapsulated material could not be removed at the end of the experiments (*3*). Modifications in the encapsulation procedure have improved the biocompatibility of the membranes by covering the poly(L-lysine) envelope with an outer layer of alginate (*4*). An intravascular device that separates the islets from the blood stream by permselective membranes was developed (*5*), but blood coagulated in the vascular lumen. An improved intravascular device maintained normoglycemia for several months in diabetic canines that had been implanted with two devices that contained canine islets (*6*).

Hollow fibers formed of poly(acrylonitrile-*co*-vinyl chloride) (Amicon XM50) have been used for encapsulation of neonatal mouse islet cells before transplantation into diabetic hamsters and for encapsulation and transplantation of human insulinoma cells into rats (*7*). The encapsulated islet tissue was transplanted into the abdominal cavity, and in each of the two studies prolongation of survival of the islet xenografts was obtained in a few animals. Studies of the biocompatibility of these fibers have revealed a slight glial reaction when implanted into the brain of rats and only one to two layers of fibroblasts surrounded by collagen in mice when implanted intraperitoneally (*8*).

We studied two types of acrylic copolymer hollow fibers to determine their efficacy in achieving normoglycemia when used for encapsulation of Wistar-Furth rat islets. Type 1 and type 2 fibers were identical except for their outer surface wall. Type 1 had a totally fenestrated outer wall, whereas type 2 fibers had a smooth outer surface (Fig. 1). Type 1 fibers were formed by the usual technique of extruding the fibers di-

P. E. Lacy and A. Gerasimidi-Vazeou, Department of Pathology, Washington University School of Medicine, St. Louis, MO 63110.
O. D. Hegre, F. T. Gentile, K. E. Dionne, Cellular Transplants, Providence, RI 02906.

*To whom correspondence should be addressed.